Article

Not peer-reviewed version

Adaptive Backstepping Control of an Unmanned Aerial Manipulator

Muhammad Awais Rafique and Alan F Lynch *

Posted Date: 27 August 2025

doi: 10.20944/preprints202508.1963.v1

Keywords: unmanned aerial vehicle (UAV); unmanned aerial manipulation (UAM); motion control; stability analysis

 doi:10.20944/preprints202508.1963.v1

Article

Adaptive Backstepping Control of an Unmanned Aerial Manipulator

Muhammad Awais Rafique and Alan F. Lynch *

Department of Electrical and Computer Engineering, University of Alberta, AB, Canada
* Correspondence: alynch@ualberta.ca

Abstract

This paper presents an adaptive backstepping feedback control design for an unmanned aerial manipulator (UAM) which consists of an unmanned aerial vehicle (UAV) with attached robotic arm. The effect of the arm is treated as a disturbance force and torque to the UAV and as parametric uncertainty in the UAV inertial parameters. The proposed adaptive law guarantees disturbance rejection assuming constant parameters and disturbances. In practice, this assumption includes the case of fixed arm configurations. To validate the control design, numerical simulations are performed, where a realistic pick-and-place scenario is presented.

Keywords: unmanned aerial vehicle (UAV); unmanned aerial manipulation (UAM); motion control; stability analysis

---

1. Introduction

Research on unmanned aerial vehicles (UAVs) has recently focussed on tasks involving manipulation of the environment. Normally, this interaction is achieved by mounting an "arm" to the UAV so that various manipulation tasks can be achieved. The combined UAV and arm system is referred to as an *unmanned aerial manipulator (UAM)*. Applications such as non-destructive testing of infrastructure require the UAM to keep a sensor in contact with the surface being inspected. The sensor must follow a desired trajectory on the surface and a predefined force must be applied.

Initial work on UAM motion control tends to focus on single-link arms which are rigidly attached to the UAV. UAM force and motion control dates back to [1], where the "arm" consists of a single rod rigidly attached to the UAV. An additional propeller is used to apply force to a surface. A heuristically designed proportional-integral-derivative (PID) controller structure is proposed, and no stability result is given for the force/motion control problem. Work in [2] provides a rigorous stability result using a nonlinear output feedback. The work assumes the single-fixed link arm does not affect the CoM of the system. The dynamics of the end-effector position is decomposed into tangential and normal directions. Error stability requires the beam to be attached "above" the UAV CoM. This work is extended in [3] where it is shown that the end-effector can generate any contact force if it is strictly located either below or above the UAV CoM. The article [4] studies the problem of UAV interaction with the environment without an arm. A'' cascade controller allows the UAV to "push" against objects using pads attached to the UAV frame. The stability analysis is based on a planar quasi-static motion assumption. This apparatus is improved in [5] where tilted propellers are used. A heuristic PID control is proposed without a formal stability result.

Feedback control for multi-DoF arm UAMs can be classified into two main approaches: (i) separate controllers for the UAV and the arm, and (ii) full UAM control. In Approach (i), the coupling forces/torques acting on the UAV due to the arm are treated as a disturbance [6–11]. Approach (i) generally leads to a simpler subsystem-at-a-time design. Approach (ii) views the entire UAM as a single coupled dynamics [12]. This approach is challenging as the entire dynamics is very complex and complexity dramatically increases with the number of arm DoF [13–17]. Hence, this paper follows

 doi:10.20944/preprints202508.1963.v1

Approach (i) and compensates for the effect of the arm by introducing uncertain inertial parameters and force/torque disturbances into a UAV dynamics.

Approach (i) is widely found in the literature e.g., [6–8]. The work of [6] considers a UAV with a 4-DoF arm. For the UAV inner-loop, i.e., attitude dynamics, a disturbance observer based on [18] is used to estimate the effect of the arm on the UAV. With these estimates, feedback control is designed for the inner-loop that compensates for the disturbance. The outer-loop is treated separately. The effect of coupling between the loops on closed-loop stability is not considered. To validate their approach on a real UAM, the UAV outer-loop controller is taken from [19]. Work in [20] uses model reference control for the UAV outer-loop *only*. The UAV mass is taken as the unknown parameter. The effect of coupling forces and torques due to the arm on the UAV is not considered. Unlike [6] and [20], our work rejects the arm disturbance while considering the *full* UAV dynamics. The article [21] considers a UAV with a 3-DoF arm. It proposes a solution for constant setpoint regulation using a Luenberger observer to estimate the torque disturbance due to the arm. Our work is not limited to regulation and designs a trajectory-tracking feedback. We remark that the literature on robust UAV control, i.e., without an arm, is related to Approach (i). Examples of this include [22,23].

In this paper, our control objective is trajectory tracking of the UAV CoM and yaw. The effect of the arm on the UAV is modelled in two ways: it adds a force and torque disturbance to the UAV and introduces parametric uncertainty e.g., arm motion alters the UAV CoM and inertia matrix. We are inspired by the work of [24,25] on UAV motion control. These contributions only consider the force and torque disturbances, while all the inertial parameters are assumed known. Our work also allows for unknown inertial UAV parameters. We propose an adaptive backstepping control scheme that is capable of compensating force/torque disturbances and parameter uncertainty. This work is based on the first author's thesis [26].

This paper is organized as follows. Section 2 presents the model of the UAM. Section 3 presents model assumptions, formulates the control problem, proposes a control design, and performs stability analysis. Numerical simulations are presented in Section 4. Finally, Section 5 concludes the paper.

2. Modelling

Consider a UAM consisting of a UAV with attached robotic arm. In this section, we present the UAV model and introduce a force/torque disturbance and parametric uncertainty to model the effect of the arm. The UAV model neglects the effects of motor dynamics, rotor drag, and the rotor gyroscopic effects. The details on modelling these higher-order effects are discussed in [27,28].

Consider Figure 1. Let $\mathcal{N}$ denote an inertial navigation frame with basis vectors $\{n_1, n_2, n_3\}$ pointing north, east, down, respectively. Let $\mathcal{B}$ denote a body-fixed frame whose origin coincides with the UAV CoM and whose basis vectors are $\{b_1, b_2, b_3\}$ and point forward, right, and downward, relative to the UAV. The position of the origin of $\mathcal{B}$ relative to the origin of $\mathcal{N}$ is denoted, $p \in \mathbb{R}$, which is expressed in $\mathcal{N}$. The linear velocity the UAV CoM, $v \in \mathbb{R}$, is given by

$$\dot{p} = v. \tag{1}$$

The orientation of $\mathcal{B}$ relative to $\mathcal{N}$ is described by the rotation matrix $R \in \mathrm{SO}(3)$. The angular velocity $\omega \in \mathbb{R}^3$ of the UAV relative to $\mathcal{N}$ expressed in $\mathcal{B}$ is related to R by

$$\dot{R} = R\mathrm{S}(\omega), \tag{2}$$

where

$$\mathrm{S}(x) = \begin{bmatrix} 0 & -x_3 & x_2 \\ x_3 & 0 & -x_1 \\ -x_2 & x_1 & 0 \end{bmatrix}, \qquad x = \begin{bmatrix} x_1 \\ x_2 \\ x_3 \end{bmatrix} \in \mathbb{R}^3.$$

The UAV input is total propeller thrust $u \in \mathbb{R}_{>0}$ which creates a force in $-b_3$ direction, and torque $\tau \in \mathbb{R}^3$ on $\mathcal{B}$. Letting $m \in \mathbb{R}$ denote UAV mass and $J \in \mathbb{R}^{3\times3}$ denote UAV inertia, the UAV dynamics is

$$\begin{aligned} m\dot{v} &= mge_3 - F, \\ J\dot{\omega} &= -\mathrm{S}(\omega)J\omega + \tau \end{aligned} \tag{3}$$

where $F = -uRe_3$, $e_3 = [0,0,1]^\top$, and g is gravitational acceleration. We remark that (3) models the UAV in isolation from the arm. To account for the effect of the arm, we introduce disturbance force $d_f \in \mathbb{R}^3$ and torque $d_\tau \in \mathbb{R}^3$ that can be interpreted as a change in input due to the arm. Further, we consider inertial parameters $a \in \mathbb{R}$ and J as uncertain:

$$\dot{p} = v, \tag{4a}$$
$$\dot{v} = ge_3 - auRe_3 + d_f, \tag{4b}$$
$$\dot{R} = R\mathrm{S}(\omega), \tag{4c}$$
$$J\dot{\omega} = -\mathrm{S}(\omega)J\omega + \tau + d_\tau. \tag{4d}$$

Further details on the UAM model simplification are in [26, Sec. 2.2.4,2.2.5].

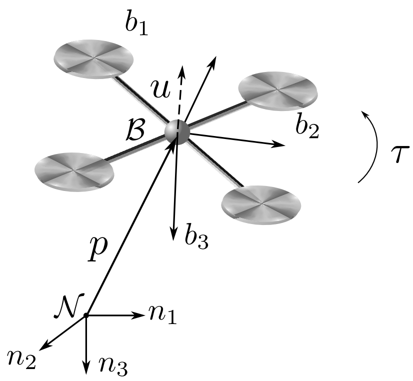

Figure 1. Diagram of a quadrotor with modelling notation.

Note that J in (4) is a positive definite symmetric matrix with six unique entries. These entries of J define the vector $J_v = [J_{xx}, J_{yy}, J_{zz}, J_{xy}, J_{yz}, J_{zx}]^\top \in \mathbb{R}^6$. Using J_v we can re-write the $\mathrm{S}(\omega)J\omega$ term in (4d) as

$$\mathrm{S}(\omega)J\omega = \Phi(\omega)J_v \tag{5}$$

where $\Phi(\omega) \in \mathbb{R}^{3\times6}$. In model (4) we take a, J_v, d_f and d_τ as unknown constants and denote $\hat{a} \in \mathbb{R} > 0$, $\hat{J}_v \in \mathbb{R}^6$, $\hat{d}_f \in \mathbb{R}^3$, and $\hat{d}_\tau \in \mathbb{R}^3$ as their estimates. Estimation errors are defined as $\tilde{a} = a - \hat{a}$, $\tilde{J}_v = J_v - \hat{J}_v$, $\tilde{d}_f = d_f - \hat{d}_f$, and $\tilde{d}_\tau = d_\tau - \hat{d}_\tau$.

3. Control Design

This section presents the control design for the UAM model (4). Figure 2 shows the structure of the proposed control, where the arm is controlled separately using a PID control. In this figure, we denote α as the arm's joint angles and their desired reference as α_d. The proposed control compensates for the effect of the arm using an adaptive backstepping design method. The control objective is trajectory tracking for UAV CoM position p and UAV heading ψ. We first present the design for tracking p and then extend it for tracking ψ.

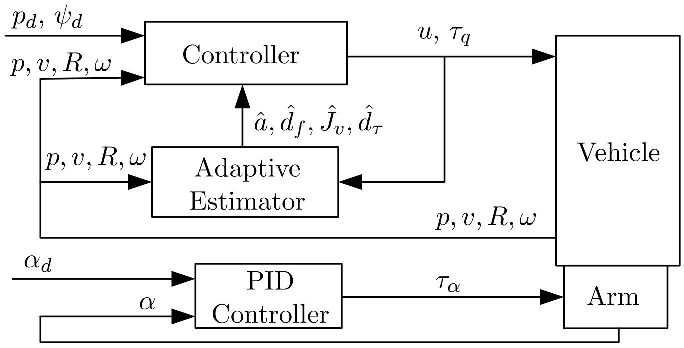

Figure 2. The proposed UAM controller structure. The control of the UAV and arm are decoupled.

3.1. Position Tracking Control

Let $p_d, v_d \in \mathbb{R}^3$ represent the desired UAV CoM position and velocity, respectively. We define error coordinate $z_1 = p - p_d$. Taking its time-derivative gives

$$\dot{z}_1 = \dot{p} - \dot{p}_d = v - v_d. \tag{6}$$

For this dynamics, consider the Lyapunov function $V_1 = \frac{1}{2} z_1^\top z_1$. Taking its time-derivative gives

$$\begin{aligned} \dot{V}_1 &= z_1^\top \dot{z}_1 \\ &= z_1^\top (v - v_d). && \text{(from (6))} \end{aligned}$$

Adding and subtracting $k_1 z_1^\top z_1$ to $\dot{V}_1$, where $k_1 > 0$ is a controller gain, we obtain

$$\dot{V}_1 = -k_1 \|z_1\|^2 + z_1^\top (v - v_d + k_1 z_1). \tag{7}$$

From (7) we define $z_2 = v - v_d + k_1 z_1$ so we can rewrite (6) as

$$\dot{z}_1 = -k_1 z_1 + z_2. \tag{8}$$

Taking the time-derivative of z_2, substituting the translational velocity dynamics from (4b), using $a = \hat{a} + \tilde{a}$, and $d_f = \hat{d}_f + \tilde{d}_f$, we arrive at

$$\dot{z}_2 = ge_3 - \hat{a}uRe_3 + \hat{d}_f - \dot{v}_d - k_1^2 z_1 + k_1 z_2 - \tilde{a}uRe_3 + \tilde{d}_f. \tag{9}$$

For the above dynamics, consider the Lyapunov function $V_2 = V_1 + \frac{1}{2} z_2^\top z_2$. Its time derivative is

$$\dot{V}_2 = \dot{V}_1 + z_2^\top \dot{z}_2$$

In this expression, substituting for $\dot{V}_1$ from (7) and for $\dot{z}_2$ from (9), and simplifying, we arrive at

$$\dot{V}_2 = -k_1 \|z_1\|^2 + z_2^\top (ge_3 - \hat{a}uRe_3 + \hat{d}_f - \dot{v}_d - k_1^2 z_1 + k_1 z_2 - \tilde{a}uRe_3 + \tilde{d}_f).$$

Adding and subtracting $k_2 z_2^\top z_2$ in the above equation, where $k_2 > 0$ is a controller gain we obtain

$$\begin{aligned} \dot{V}_2 = &- k_1 \|z_1\|^2 - k_2 \|z_2\|^2 + z_2^\top (ge_3 - \hat{a}uRe_3 + \hat{d}_f - \dot{v}_d + (1 - k_1^2) z_1 \\ &+ (k_1 + k_2) z_2) - \tilde{a} z_2^\top uRe_3 + \tilde{d}_f^\top z_2. \end{aligned} \tag{10}$$

In the above equation, we define the coefficient of $z_2^\top$ as

$$z_3 = ge_3 - \hat{a}uRe_3 + \hat{d}_f - \dot{v}_d + (1 - k_1^2) z_1 + (k_1 + k_2) z_2, \tag{11}$$

which can be rearranged as

$$z_3 - z_1 - k_2 z_2 = g e_3 - \hat{a} u R e_3 + \hat{d}_f - \dot{v}_d - k_1^2 z_1 + k_1 z_2.$$

Substituting this into (9) gives

$$\dot{z}_2 = z_3 - z_1 - k_2 z_2 - \tilde{a} u R e_3 + \tilde{d}_f. \tag{12}$$

The time-derivative of (11) is

$$\dot{z}_3 = -\dot{\hat{a}} u R e_3 - \hat{a} \dot{u} R e_3 - \hat{a} u \dot{R} e_3 + \dot{\hat{d}}_f - \ddot{v}_d + (1 - k_1^2)\dot{z}_1 + (k_1 + k_2)\dot{z}_2.$$

Substituting (8) and (12) into the last equation, we get

$$\begin{aligned}\dot{z}_3 = &- \dot{\hat{a}} u R e_3 - \hat{a} \dot{u} R e_3 - \hat{a} u R S(\omega) e_3 + \dot{\hat{d}}_f - \ddot{v}_d + (1 - k_1^2)(-k_1 z_1 + z_2) \\ &+ (k_1 + k_2)(z_3 - z_1 - k_2 z_2 - \tilde{a} u R e_3 + \tilde{d}_f).\end{aligned}$$

Simplifying leads us to

$$\begin{aligned}\dot{z}_3 = &- \dot{\hat{a}} u R e_3 - \hat{a} \dot{u} R e_3 - \hat{a} u R S(\omega) e_3 + \dot{\hat{d}}_f - \ddot{v}_d \\ &+ (k_1(k_1^2 - 1) - k_2 - k_1) z_1 + (1 - k_2(k_1 + k_2) - k_1^2) z_2 \\ &+ (k_1 + k_2) z_3 - (k_1 + k_2)\tilde{a} u R e_3 + (k_1 + k_2)\tilde{d}_f.\end{aligned} \tag{13}$$

For the above dynamics, consider the Lyapunov function $V_3 = V_2 + \frac{1}{2} z_3^\top z_3$ whose time-derivative is

$$\dot{V}_3 = -k_1 \|z_1\|^2 - k_2 \|z_2\|^2 + z_2^\top z_3 + z_3^\top \dot{z}_3 - \tilde{a} z_2^\top u R e_3 + \tilde{d}_f^\top z_2.$$

Substituting (13) in the last equation leads to

$$\begin{aligned}\dot{V}_3 = &- k_1 \|z_1\|^2 - k_2 \|z_2\|^2 + z_3^\top \big(z_2 - \dot{\hat{a}} u R e_3 - \hat{a} \dot{u} R e_3 - \hat{a} u R S(\omega) e_3 + \dot{\hat{d}}_f - \ddot{v}_d \\ &+ (k_1(k_1^2 - 1) - k_2 - k_1) z_1 + (1 - k_2(k_1 + k_2) - k_1^2) z_2 + (k_1 + k_2) z_3 \\ &- (k_1 + k_2)\tilde{a} u R e_3 + (k_1 + k_2)\tilde{d}_f\big) - \tilde{a} z_2^\top u R e_3 + \tilde{d}_f^\top z_2.\end{aligned}$$

Adding and subtracting $k_3 z_3^\top z_3$ from the last expression, where $k_3 > 0$ is a controller gain, and simplifying gives

$$\begin{aligned}\dot{V}_3 = &- k_1 \|z_1\|^2 - k_2 \|z_2\|^2 - k_3 \|z_3\|^2 + z_3^\top \big(- \dot{\hat{a}} u R e_3 - \hat{a} \dot{u} R e_3 - \hat{a} u R S(\omega) e_3 + \dot{\hat{d}}_f \\ &- \ddot{v}_d + (k_1(k_1^2 - 1) - k_2 - k_1) z_1 + (2 - k_2(k_1 + k_2) - k_1^2) z_2 + (k_1 + k_2 + k_3) z_3\big) \\ &- \tilde{a}(z_2^\top + (k_1 + k_2) z_3^\top) u R e_3 + \tilde{d}_f^\top (z_2 + (k_1 + k_2) z_3).\end{aligned}$$

Now, consider a modified Lyapunov function

$$V_{3b} = V_3 + \frac{1}{2\lambda}\tilde{a}^2 + \frac{1}{2k_{d_f}}\tilde{d}_f^\top \tilde{d}_f, \tag{14}$$

where $k_{d_f} > 0, \lambda > 0$ are controller gains. The time-derivative of V_{3b} is

$$\begin{aligned}\dot{V}_{3b} = &- k_1 \|z_1\|^2 - k_2 \|z_2\|^2 - k_3 \|z_3\|^2 + z_3^\top \big(- \dot{\hat{a}} u R e_3 - \hat{a} \dot{u} R e_3 - \hat{a} u R S(\omega) e_3 + \dot{\hat{d}}_f \\ &- \ddot{v}_d + (k_1(k_1^2 - 1) - k_2 - k_1) z_1 + (2 - k_2(k_1 + k_2) - k_1^2) z_2 + (k_1 + k_2 + k_3) \\ &\times z_3\big) - \tilde{a}(z_2^\top + (k_1 + k_2) z_3^\top) u R e_3 + \tilde{d}_f^\top (z_2 + (k_1 + k_2) z_3) + \frac{1}{\lambda}\tilde{a}\dot{\tilde{a}} + \frac{1}{k_{d_f}}\tilde{d}_f^\top \dot{\tilde{d}}_f.\end{aligned}$$

Preprints.org (www.preprints.org) | NOT PEER-REVIEWED | Posted: 27 August 2025 doi:10.20944/preprints202508.1963.v1

With some simplification, we get

$$\begin{aligned}\dot{V}_{3b} =& -k_1\|z_1\|^2 - k_2\|z_2\|^2 - k_3\|z_3\|^2 + z_3^\top\big(-\dot{\hat{a}}uRe_3 - \hat{a}\dot{u}Re_3 - \hat{a}uRS(\omega)e_3 \\ &+ \dot{\hat{d}}_f - \ddot{v}_d + (k_1(k_1^2-1) - k_2 - k_1)z_1 + (2 - k_2(k_1+k_2) - k_1^2)z_2 \\ &+ (k_1+k_2+k_3)z_3\big) + \tilde{a}\big(\lambda\dot{\hat{a}} - (z_2^\top + (k_1+k_2)z_3^\top)uRe_3\big) \\ &+ \tilde{d}_f^\top\big(\frac{1}{k_{d_f}}\dot{\hat{d}}_f + z_2 + (k_1+k_2)z_3\big).\end{aligned} \tag{15}$$

We define $\sigma_1, \sigma_2 \in \mathbb{R}^3$ to re-write (15):

$$\sigma_1 =(k_1(k_1^2-1) - k_2 - k_1)z_1 + (2 - k_2(k_1+k_2) - k_1^2)z_2 + (k_1+k_2+k_3)z_3 - \ddot{v}_d, \tag{16a}$$

$$\sigma_2 =z_2 + (k_1+k_2)z_3. \tag{16b}$$

Since d_f is constant, we have $\dot{\tilde{d}}_f = -\dot{\hat{d}}_f$. Substituting this equation in (15) and using the definitions of σ_1, σ_2, we obtain

$$\begin{aligned}\dot{V}_{3b} =& -k_1\|z_1\|^2 - k_2\|z_2\|^2 - k_3\|z_3\|^2 + z_3^\top\big(-\dot{\hat{a}}uRe_3 - \hat{a}\dot{u}Re_3 \\ &- \hat{a}uRS(\omega)e_3 + \dot{\hat{d}}_f + \sigma_1\big) + \tilde{a}\big(\frac{1}{\lambda}\dot{\tilde{a}} - \sigma_2^\top uRe_3\big) + \tilde{d}_f^\top\big(-\frac{1}{k_{d_f}}\dot{\tilde{d}}_f + \sigma_2\big).\end{aligned}$$

Adding and subtracting $k_{d_f} z_3^\top \sigma_2$ yields

$$\begin{aligned}\dot{V}_{3b} =& -k_1\|z_1\|^2 - k_2\|z_2\|^2 - k_3\|z_3\|^2 + z_3^\top\big(-\dot{\hat{a}}uRe_3 - \hat{a}\dot{u}Re_3 - \hat{a}uRS(\omega)e_3 \\ &+ \dot{\hat{d}}_f - k_{d_f}\sigma_2 + k_{d_f}\sigma_2 - \ddot{v}_d + \sigma_1\big) + \tilde{a}\big(\frac{1}{\lambda}\dot{\tilde{a}} - \sigma_2^\top uRe_3\big) + \tilde{d}_f^\top\big(-\frac{1}{k_{d_f}}\dot{\tilde{d}}_f + \sigma_2\big),\end{aligned}$$

and simplification gives

$$\begin{aligned}\dot{V}_{3b} =& -k_1\|z_1\|^2 - k_2\|z_2\|^2 - k_3\|z_3\|^2 + z_3^\top(-\dot{\hat{a}}uRe_3 - \hat{a}\dot{u}Re_3 \\ &- \hat{a}uRS(\omega)e_3 + \sigma_1 + k_{d_f}\sigma_2) - k_{d_f}z_3^\top\big(-\frac{1}{k_{d_f}}\dot{\tilde{d}}_f + \sigma_2\big) \\ &+ \tilde{a}\big(\frac{1}{\lambda}\dot{\tilde{a}} - \sigma_2^\top uRe_3\big) + \tilde{d}_f^\top\big(-\frac{1}{k_{d_f}}\dot{\tilde{d}}_f + \sigma_2\big).\end{aligned} \tag{17}$$

Observe

$$\begin{aligned}\sigma_1 + k_{d_f}\sigma_2 =& RR^\top(\sigma_1 + k_{d_f}\sigma_2) = RIR^\top(\sigma_1 + k_{d_f}\sigma_2) \\ =& R(I - e_3e_3^\top + e_3e_3^\top)R^\top(\sigma_1 + k_{d_f}\sigma_2) \\ =& \big(R(I - e_3e_3^\top)R^\top + Re_3e_3^\top R^\top\big)(\sigma_1 + k_{d_f}\sigma_2).\end{aligned}$$

Hence,

$$\begin{aligned}\dot{V}_{3b} =& -k_1\|z_1\|^2 - k_2\|z_2\|^2 - k_3\|z_3\|^2 + z_3^\top\big(-\dot{\hat{a}}uRe_3 - \hat{a}\dot{u}Re_3 \\ &+ Re_3e_3^\top R^\top(\sigma_1 + k_{d_f}\sigma_2) - \hat{a}uRS(\omega)e_3 + R(I - e_3e_3^\top)R^\top(\sigma_1 + k_{d_f}\sigma_2)\big) \\ &- k_{d_f}z_3^\top\big(-\frac{1}{k_{d_f}}\dot{\tilde{d}}_f + \sigma_2\big) + \tilde{a}\big(\frac{1}{\lambda}\dot{\tilde{a}} - \sigma_2^\top uRe_3\big) + \tilde{d}_f^\top\big(-\frac{1}{k_{d_f}}\dot{\tilde{d}}_f + \sigma_2\big).\end{aligned}$$

Let's factor out Re_3 from the first three terms inside the parentheses of the $z_3^\top$ coefficient and equate them to zero. In other words, let's impose $\hat{a}\dot{u} + \dot{\hat{a}}u - e_3^\top R^\top(\sigma_1 + k_{d_f}\sigma_2) = 0$, which gives

$$\hat{a}\dot{u} + \dot{\hat{a}}u = e_3^\top R^\top(\sigma_1 + k_{d_f}\sigma_2). \tag{18}$$

Therefore,

$$
\begin{aligned}
\dot{V}_{3b} =& -k_1\|z_1\|^2 - k_2\|z_2\|^2 - k_3\|z_3\|^2 + z_3^\top R\big(-\hat{a}u\mathrm{S}(\omega)e_3 \\
&+ (I - e_3e_3^\top)R^\top(\sigma_1 + k_{d_f}\sigma_2)\big) + (\tilde{d}_f^\top - k_{d_f}z_3^\top)(-\frac{1}{k_{d_f}}\dot{\hat{d}}_f + \sigma_2) \\
&+ \tilde{a}(\frac{1}{\lambda}\dot{\hat{a}} - \sigma_2^\top uRe_3).
\end{aligned} \tag{19}
$$

The term $\hat{a}u\mathrm{S}(\omega_d)e_3$ in (19) can be interpreted as a virtual control, whose desired value is taken as

$$\hat{a}u\mathrm{S}(\omega_d)e_3 = (I - e_3e_3^\top)R^\top(\sigma_1 + k_{d_f}\sigma_2).$$

Since $\mathrm{S}(\omega_d)e_3 = -\mathrm{S}(e_3)\omega_d$, the last equation can be rewritten as

$$\hat{a}u\mathrm{S}(e_3)\omega_d = -(I - e_3e_3^\top)R^\top(\sigma_1 + k_{d_f}\sigma_2). \tag{20}$$

Extracting individual components of ω_d, we have

$$\omega_{d1} = -\frac{e_2^\top}{\hat{a}u}(I - e_3e_3^\top)R^\top(\sigma_1 + k_{d_f}\sigma_2), \tag{21}$$

$$\omega_{d2} = \frac{e_1^\top}{\hat{a}u}(I - e_3e_3^\top)R^\top(\sigma_1 + k_{d_f}\sigma_2), \tag{22}$$

while (19) becomes

$$
\begin{aligned}
\dot{V}_{3b} =& -k_1\|z_1\|^2 - k_2\|z_2\|^2 - k_3\|z_3\|^2 + z_3^\top\big(-\hat{a}uR\mathrm{S}(\omega)e_3 + \hat{a}uR\mathrm{S}(\omega_d)e_3\big) \\
&+ (\tilde{d}_f^\top - k_{d_f}z_3^\top)(-\frac{1}{k_{d_f}}\dot{\hat{d}}_f + \sigma_2) + \tilde{a}(\frac{1}{\lambda}\dot{\hat{a}} - \sigma_2^\top uRe_3).
\end{aligned}
$$

Simplifying the last expression gives

$$
\begin{aligned}
\dot{V}_{3b} =& -k_1\|z_1\|^2 - k_2\|z_2\|^2 - k_3\|z_3\|^2 + z_3^\top\hat{a}uR\mathrm{S}(e_3)\big(\omega - \omega_d\big) \\
&+ (\tilde{d}_f^\top - k_{d_f}z_3^\top)(-\frac{1}{k_{d_f}}\dot{\hat{d}}_f + \sigma_2) + \tilde{a}(\frac{1}{\lambda}\dot{\hat{a}} - \sigma_2^\top uRe_3).
\end{aligned} \tag{23}
$$

Now, consider the following parameter update laws,

$$
\begin{aligned}
\dot{\hat{d}}_f =& k_{d_f}\sigma_2, \\
\dot{\hat{a}} =& -\lambda\sigma_2^\top uRe_3,
\end{aligned} \tag{24}
$$

Substituting these adaptive laws in (23), we have

$$\dot{V}_{3b} = -k_1\|z_1\|^2 - k_2\|z_2\|^2 - k_3\|z_3\|^2 + z_3^\top\hat{a}uR\mathrm{S}(e_3)\big(\omega - \omega_d\big). \tag{25}$$

Let the error in angular velocity be $z_4 = \omega - \omega_d$. Using (4d), we can write

$$J\dot{z}_4 = J\dot{\omega} - J\dot{\omega}_d = -\mathrm{S}(\omega)J\omega + \tau + d_\tau - J\dot{\omega}_d. \tag{26}$$

Define

$$
\begin{aligned}
\bar{\omega}_d =& -\frac{1}{\hat{a}u}(\dot{\hat{a}}u + \hat{a}\dot{u})(I - e_3e_3^T)\omega_d + \frac{1}{\hat{a}u}\mathrm{S}^\top(e_3)\mathrm{S}(\omega)R^T(\sigma_1 + k_{d_f}\sigma_2) \\
&- \frac{1}{\hat{a}u}\mathrm{S}^\top(e_3)R^T(\bar{\sigma}_1 + k_{d_f}\bar{\sigma}_2) + \dot{\omega}_{d3}e_3,
\end{aligned}
$$

Using J_v instead of J, we have

$$J\bar{\omega}_d = \Psi(\bar{\omega}_d)J_v, \tag{27}$$

 doi:10.20944/preprints202508.1963.v1

where

$$\Psi(\bar{\omega}_d) = \begin{bmatrix} \bar{\omega}_{d1} & 0 & 0 & \bar{\omega}_{d2} & 0 & \bar{\omega}_{d3} \\ 0 & \bar{\omega}_{d2} & 0 & \bar{\omega}_{d1} & \bar{\omega}_{d3} & 0 \\ 0 & 0 & \bar{\omega}_{d3} & 0 & \bar{\omega}_{d2} & \bar{\omega}_{d1} \end{bmatrix},$$

Therefore, (26) can be rewritten as

$$J\dot{z}_4 = -(\Phi(\omega) + \Psi(\dot{\omega}_d))J_v + \tau + d_\tau. \tag{28}$$

Substituting $J_v = \hat{J}_v + \tilde{J}_v$ and $d_\tau = \hat{d}_\tau + \tilde{d}_\tau$ in (28) gives

$$J\dot{z}_4 = -(\Phi(\omega) + \Psi(\dot{\omega}_d))(\hat{J}_v + \tilde{J}_v) + \tau + \hat{d}_\tau + \tilde{d}_\tau. \tag{29}$$

Now, consider the Lyapunov function

$$V_4 = V_{3b} + \frac{1}{2}z_4^\top J z_4 + \frac{1}{2k_{d_\tau}}\tilde{d}_\tau^\top \tilde{d}_\tau + \frac{1}{2}\tilde{J}_v^\top \Gamma^{-1}\tilde{J}_v, \tag{30}$$

where $k_{d_\tau} > 0$, $\Gamma \in \mathbb{R}^{6\times 6} > 0$ are controller gains. Differentiating the above equation with respect to time gives

$$\dot{V}_4 = \dot{V}_{3b} + z_4^\top J\dot{z}_4 + \frac{1}{k_{d_\tau}}\tilde{d}_\tau^\top \dot{\tilde{d}}_\tau + \tilde{J}_v^\top \Gamma^{-1}\dot{\tilde{J}}_v. \tag{31}$$

Substituting (25) and (29) into (31) gives

$$\begin{aligned} \dot{V}_4 =& -k_1\|z_1\|^2 - k_2\|z_2\|^2 - k_3\|z_3\|^2 + z_3^\top \hat{a}uRS(e_3)z_4 \\ &+ z_4^\top(-(\Phi(\omega) + \Psi(\dot{\omega}_d))(\hat{J}_v + \tilde{J}_v) + \tau + \hat{d}_\tau + \tilde{d}_\tau) \\ &+ \frac{1}{k_{d_\tau}}\tilde{d}_\tau^\top \dot{\tilde{d}}_\tau + \tilde{J}_v^\top \Gamma^{-1}\dot{\tilde{J}}_v. \end{aligned} \tag{32}$$

Let $k_4 > 0$ be a controller gain. Adding and subtracting $k_4 z_4^\top z_4$ in the above expression, factoring $z_4^\top$, we obtain

$$\begin{aligned} \dot{V}_4 =& -k_1\|z_1\|^2 - k_2\|z_2\|^2 - k_3\|z_3\|^2 - k_4\|z_4\|^2 \\ &+ z_4^\top(\hat{a}u{R_b^n}^\top S^\top(e_3)z_3 + k_4 z_4 - (\Phi(\omega) + \Psi(\dot{\omega}_d))\hat{J}_v + \tau + \hat{d}_\tau) \\ &+ \tilde{J}_v^\top(\Gamma^{-1}\dot{\tilde{J}}_v - (\Phi(\omega) + \Psi(\dot{\omega}_d))^\top z_4) + \tilde{d}_\tau^\top(\frac{1}{k_{d_\tau}}\dot{\tilde{d}}_\tau + z_4). \end{aligned} \tag{33}$$

At this point, we assign the expression for input τ:

$$\tau = -\hat{a}u{R_b^n}^\top S^\top(e_3)z_3 - k_4 z_4 + (\Phi(\omega) + \Psi(\dot{\omega}_d))\hat{J}_v - \hat{d}_\tau, \tag{34}$$

and define the parameter update laws

$$\begin{aligned} \dot{\hat{J}}_v =& -\Gamma(\Phi(\omega) + \Psi(\dot{\omega}_d))^\top z_4, \\ \dot{\hat{d}}_\tau =& k_{d_\tau} z_4. \end{aligned} \tag{35}$$

Substituting (34) and (35) in (33), and recalling that J_v and d_τ are constants, we get

$$\dot{V}_4 = -k_1\|z_1\|^2 - k_2\|z_2\|^2 - k_3\|z_3\|^2 - k_4\|z_4\|^2, \tag{36}$$

which is negative semi-definite.

Theorem 1. *Consider the UAM dynamics (4) and assume $\dot{a} = 0$, $\dot{d}_f = 0$, $\dot{d}_\tau = 0$, $\dot{J}_v = 0$, and $u > 0$, $\hat{a} > 0$. Given a smooth time-varying trajectory $p_d(t)$, feedback law (34) with $k_1, k_2, k_3, k_4 > 0$, and parameter update* *laws (24), (35), then the tracking error* $z^\top = [z_1^\top, z_2^\top, z_3^\top, z_4^\top]$ *is globally asymptotically convergent to* 0 *and parameter estimates* $\hat{a}, \hat{d}_f, \hat{d}_\tau$ *and* $\hat{J}_v$ *are bounded.*

Proof. Consider the quadratic positive definite Lyapunov function V_4 in (30). According to [29, Lemma 4.3], there exist two positive definite functions that lower and upper bound V_4. The time-derivative of V_4 after substitution of (34), (24), (35), is a negative semi-definite function. Using Barbalat's lemma [29, Theorem 8.4], we can conclude $z \to 0$ as $t \to \infty$, and parameter and disturbance estimates $\hat{a}$, $\hat{d}_f$, $\hat{d}_\tau$ and $\hat{J}_v$ are bounded. Since V_4 is radially unbounded, we conclude that the equilibrium point $z = 0$ is globally asymptotically stable. □

3.2. Position and Yaw Tracking Control

Thus far, the adaptive backstepping control design achieves trajectory tracking for p. Since the UAV has 4 control inputs, we can extend the control to track UAV heading, which is practically relevant for manipulation tasks. We identify UAV heading with yaw angle $\psi \in (-\pi, \pi]$. Let the desired UAV yaw trajectory be $\psi_d \in (-\pi, \pi]$ and define tracking error $z_\psi = \psi - \psi_d$. Let

$$V_\psi = \frac{1}{2} z_\psi^2. \tag{37}$$

Thus,

$$\dot{V}_\psi = z_\psi \dot{z}_\psi = z_\psi (\dot{\psi} - \dot{\psi}_d)$$

It can be computed that $\dot{\psi} = e_3^\top W^{-1} \omega$, where for 3-2-1 Euler angles parameterization, we have

$$W = \begin{bmatrix} 1 & 0 & -\sin\theta \\ 0 & \cos\phi & \sin\phi\cos\theta \\ 0 & -\sin\phi & \cos\phi\cos\theta \end{bmatrix}$$

and θ, ϕ represent UAV pitch, roll, respectively. Therefore, we can write

$$\dot{V}_\psi = z_\psi \dot{z}_\psi = z_\psi (e_3^\top W^{-1} \omega - \dot{\psi}_d)$$

Adding and subtracting $k_\psi z_\psi^2$, where $k_\psi > 0$ is a control gain, gives

$$\dot{V}_\psi = -k_\psi z_\psi^2 + z_\psi (k_\psi z_\psi + e_3^\top W^{-1} \omega - \dot{\psi}_d) \tag{38}$$

Define

$$e_3^\top W^{-1} \omega_d = -k_\psi z_\psi + \dot{\psi}_d \tag{39}$$

which gives

$$\omega_{d3} = \frac{c_\theta}{c_\phi} (-k_\psi z_\psi + \dot{\psi}_d + \frac{s_\phi}{c_\theta} \omega_{d2}), \tag{40}$$

where ω_{d2} is given in (22). Substituting (39) in (38) results in

$$\begin{aligned} \dot{V}_\psi &= -k_\psi z_\psi^2 + z_\psi (e_3^\top W^{-1} (\omega - \omega_d)) \\ &= -k_\psi z_\psi^2 + z_4^\top z_\psi W^{-1^\top} e_3. \end{aligned} \tag{41}$$

We are now ready to state the stability result for the position-yaw tracking controller.

Theorem 2. *Consider the UAM dynamics (4) and assuming* $\dot{a} = 0$, $\dot{d}_f = 0$, $\dot{d}_\tau = 0$ *and* $\dot{J}_v = 0$ *and* $u > 0$, $\hat{a} > 0$. *Given a smooth trajectory* $p_d(t), \psi_d(t)$, *control (18) and*

$$\tau = -z_\psi W^{-T} e_3 - \hat{a} u R_b^{n\top} S^\top(e_3) z_3 - k_4 z_4 + (\Phi(\omega) + \Psi(\dot{\omega}_d)) \hat{J}_v - \hat{d}_\tau \tag{42}$$

with $k_1 > 0, k_2 > 0, k_3 > 0, k_4 > 0$, *and parameter update laws* (24),(35), *then tracking error* $z^\top = [z_1^\top, z_2^\top, z_3^\top, z_4^\top, z_\psi]$ *converges asymptotically to* 0 *while estimates* $\hat{a}, \hat{d}_f, \hat{d}_\tau$ *and* $\hat{J}_v$ *are bounded.*

Proof. Consider the Lypunov function $V_{4,\psi} = V_4 + V_\psi$ with time derivative

$$\dot{V}_{4,\psi} = \dot{V}_4 + \dot{V}_{\psi,1}. \tag{43}$$

Substituting for $\dot{V}_4$ using (33), using parameter update laws (35), and the expression for $\dot{V}_\psi$ in (41), gives

$$\begin{aligned}\dot{V}_{4,\psi} =& -k_1\|z_1\|^2 - k_2\|z_2\|^2 - k_3\|z_3\|^2 - k_4\|z_4\|^2 - k_\psi z_\psi^2 + z_4^\top z_\psi W^{-1^\top} e_3 \\ &+ z_4^\top(\hat{a}uR_b^{n^\top} S^\top(e_3)z_3 + k_4 z_4 - (\Phi(\omega) + \Psi(\dot{\omega}_d))\hat{J}_v + \tau + \hat{d}_\tau)\end{aligned} \tag{44}$$

Substituting (42) gives

$$\dot{V}_{4,\psi} = -k_1\|z_1\|^2 - k_2\|z_2\|^2 - k_3\|z_3\|^2 - k_4\|z_4\|^2 - k_\psi\|z_\psi\|^2 \tag{45}$$

which is negative semi-definite. As in the proof of Theorem 1, we conclude $z \to 0$ as $t \to \infty$ and parameters remain bounded. □

Remark 1. *The controllers presented in* (34) *and* (42) *depend on* $\dot{\omega}_d$, *however, the above derivation gives expression for* ω_d. *The value of* $\dot{\omega}_d$ *can be obtained numerically by low-pass filtered finite difference. The algebraic expression for* ω_d *depends on* $\dot{d}_f$ *which is not known. As well, the unknown inertia vector* J_v *in the angular velocity dynamics makes the stability result difficult to prove. Work in [26] provides further details for alternate solutions to this problem.*

4. Simulation Results

This section presents numerical simulations using MATLAB Simscape Multibody to validate our control design. The files to generate these simulations can be found at https://github.com/ANCL/UAM_control. A multibody simulation is necessary to avoid the complexity of simulating the closed-loop in a traditional state-space format. The UAM used in the simulation is shown in Figure 3. The arm is a 3-link 2-DoF manipulator with two revolute joints. Link 1 is attached to the CoM of the UAV and rotates in the $b_1 - b_3$ plane about the origin of $\mathcal{B}$. Link 2 is a revolute joint which also rotates in the same plane. Link 3 is fixed to Link 2 and acts as a payload mass. The arm parameters are given in Table 2. The UAV parameters are given in Table 1. We consider three simulations: a figure-8 desired position with fixed and moving arm cases, and a pick and place operation.

Table 1. UAV parameters.

Parameter	Value	Parameter	Value
m	1.6 kg	J_{xx}, J_{yy}	0.03 kg m^2
J_{zz}	0.05 kg m^2	J_{xy}, J_{zx}, J_{yz}	0.0 kg m^2

Table 2. Arm parameters.

Parameter	Link 1	Link 2	Link 3
Joint Type	Revolute	Revolute	Fixed
Mass (kg)	0.1	0.1	0.1
Length (m)	0.2	0.3	0.1
Inertia (kg m^2)	$[7.508, 7.533, 0.0417] \times 10^{-4}$	$[7.508, 7.533, 0.0417] \times 10^{-4}$	$[1.667, 1.667, 1.667] \times 10^{-4}$

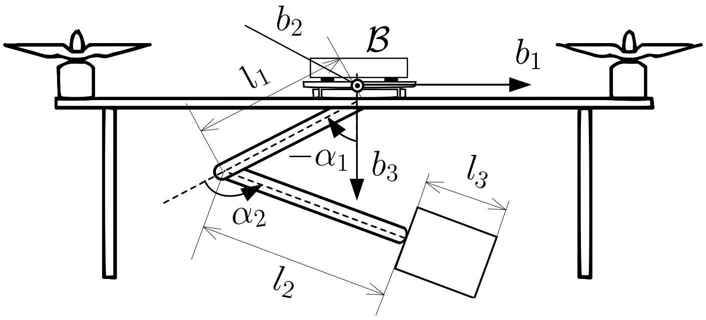

Figure 3. UAM Configuration.

4.1. Figure-8 Reference Trajectory

For the figure-8 trajectory, in addition to the coupling forces and torques due to the arm, we consider a constant external disturbance force of $[0.3, 0.3, 0.3]^\top$N acting at the UAV CoM. The controller gains used for all simulations are in Table 3. Initial conditions are $p(0) = [-2, 2, 0]^\top$ m, $v(0) = 0\,\mathrm{m\,s^{-1}}$, $\eta(0) = 0$ rad and $\omega(0) = 0\,\mathrm{rad\,s^{-1}}$, $\hat{a}(0) = \frac{1}{0.7m}$, and $\hat{J}_v(0) = 0.6J_v$ i.e., we consider a 30% error in mass and a 40% error in inertia initially. The initial conditions for the disturbances are $\hat{d}_f(0) = \hat{d}_\tau(0) = 0$.

Table 3. Control Gains

Parameter	Value	Parameter	Value
k_1	0.4	k_2	0.5
k_3	0.5	k_4	7
k_{d_f}	1	λ	3
Γ	0.001	k_{d_τ}	5
k_ψ	1		

Figures 4(a)-4(f) present the simulation results for the fixed arm case $\alpha_1 = \alpha_2 = 0$ where the arm is locked in the b_3 direction. The position tracking errors in Figure 4(b) converge to a small neighbourhood of 0. Estimates $\hat{a}$, $\hat{d}_f$, $\hat{d}_\tau$, $\hat{J}_v$ remain bounded. These estimates are shown in Figures 4(c), 4(d), and 4(e). We observe that in steady-state these parameters are time-varying due to the time-varying reference trajectory. That is, the UAV must vary its attitude to track the position trajectory, and this creates a time-varying disturbance. Increasing controller gains leads to faster tracking error convergence and smaller ultimate error bounds caused by time-varying disturbances. Figure 4(f) shows the control inputs.

The simulation results for the moving arm case are given in Figures 5(a)-5(f). The arm motion is taken as $\alpha_1(t) = \frac{\pi}{3}\sin(\pi t)$ and $\alpha_2(t) = \frac{3\pi}{2}t$. Figure 5(b) shows the UAV CoM position errors, which admit small oscillations around the origin. Relative to the fixed arm case, we observe larger error in steady-state. However, from a practical perspective, the error is not significant. The estimated parameters and disturbances are bounded and shown in Figures 5(c), 5(d), and 5(e). As in the fixed arm case, these parameters are time-varying in steady state, and large variations are observed. Figure 5(f) shows the control inputs.

We now present a practical pick and place motion where the UAM takes off to a target position, extends its arm, picks up a payload, flies to a desired location, and places the payload at the desired location. Multiple "table" landmarks are created in MATLAB Simscape Multibody that correspond to the various locations of the task. A small cubic payload of mass 0.1kg and dimension 0.1m is attached to the end-effector. The UAV CoM start location is $p(0) = [-2, 2, 0]^\top$m. The first and second desired UAV CoM positions and yaw are denoted Location 1 and Location 2, respectively. Location 1 is $p_d^1 = [1.4379, 2.0000, -1.4121]^\top$m, $\psi_d^1 = 0$ rad and Location 2 is $p_d^2 = [-2, -1.4379, -0.9121]^\top$m, $\psi_d^2 = -\pi/2$ rad. When picking up the payload, the UAV position is lowered using a function $h(t_0) = [0, 0, 0.1\sin(\pi(t_0)/5))]^\top$. Table 4 shows the desired trajectory for the UAV and arm. The Home configuration for the arm is selected to be $\alpha_1 = -\pi/4, \alpha_2 = 3\pi/4$. The desired values of p and ψ are shown in Figure 6(**a**). The position errors are given in Figure 6(**b**). The figures label each phase of the task. Evidently, the figures show tracking error is asymptotically convergent as expected by the theory. In this task, the assumptions of Theorem 2 hold as desired position and arm configuraiton is eventualy constant. Hence, this simulation case illustrates a practical case where assumptions hold.

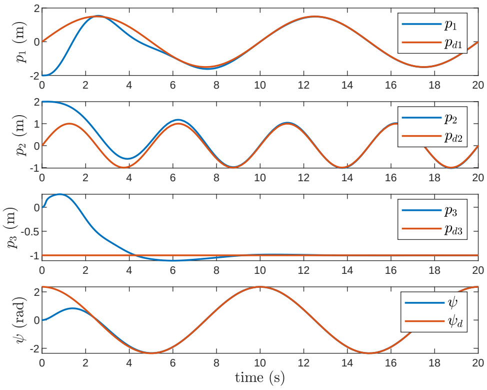

(**a**) Trajectories for p, ψ

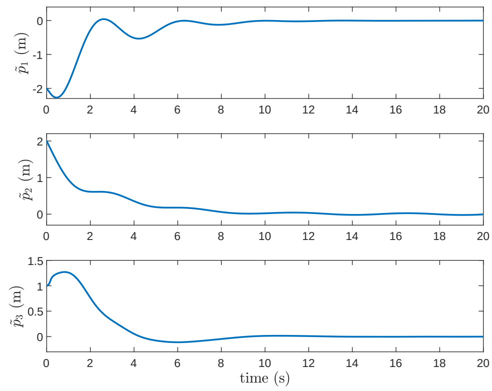

(**b**) Position error $\tilde{p}$

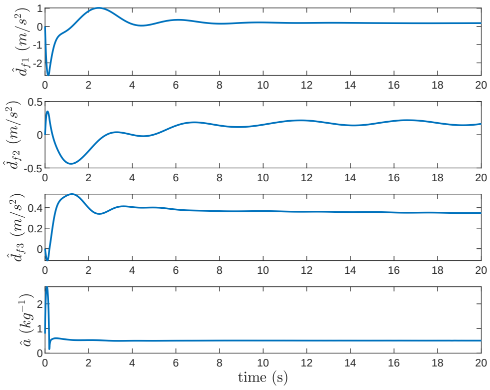

(**c**) Parameter estimates $\hat{d}_f, \hat{a}$

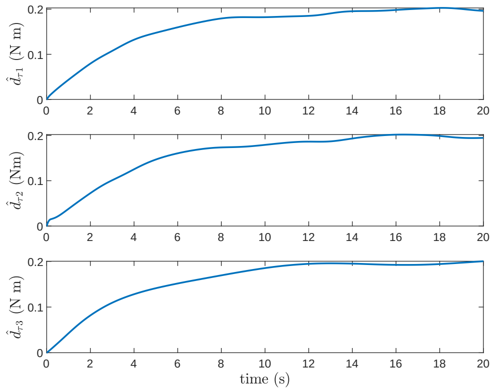

(**d**) Parameter estimates $\hat{d}_\tau$

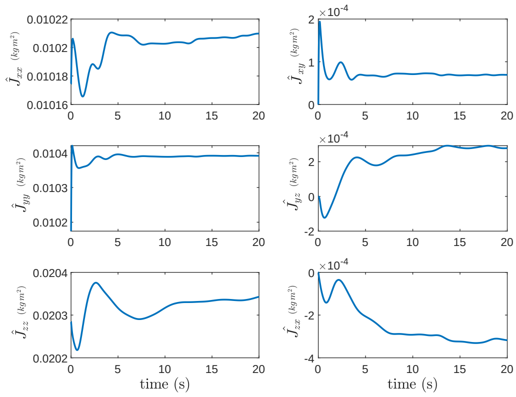

(**e**) Parameter estimates $\hat{J}$

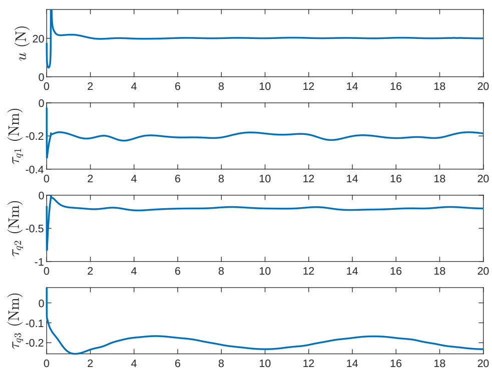

(**f**) Inputs u, τ

Figure 4. Results for fixed arm configuration ($\alpha_1 = \alpha_2 = 0$).

Preprints.org (www.preprints.org) | NOT PEER-REVIEWED | Posted: 27 August 2025 doi:10.20944/preprints202508.1963.v1

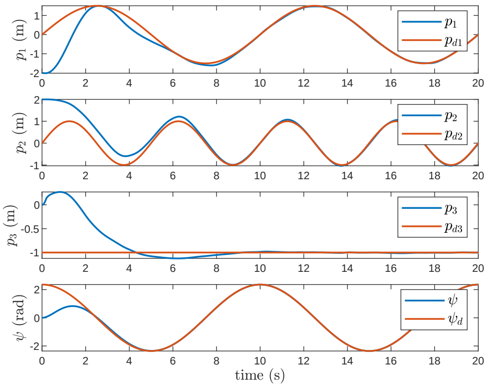

(**a**) Trajectories for p, ψ

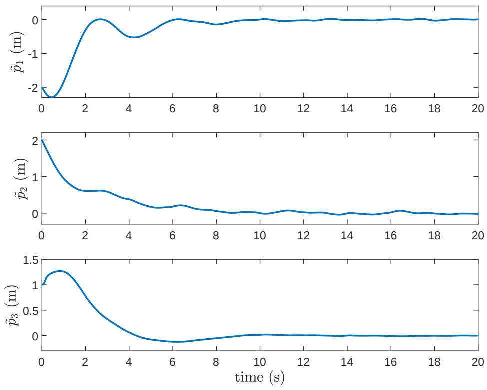

(**b**) Position tracking error $\tilde{p}$

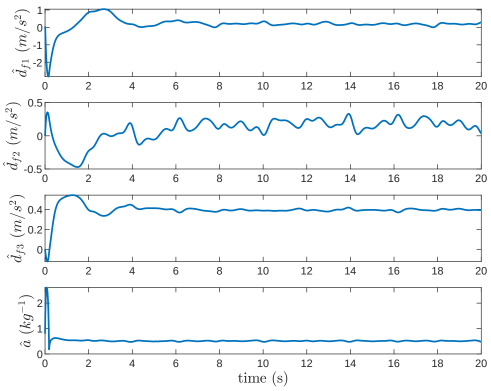

(**c**) Parameter estimates $\hat{d}_f, \hat{a}$

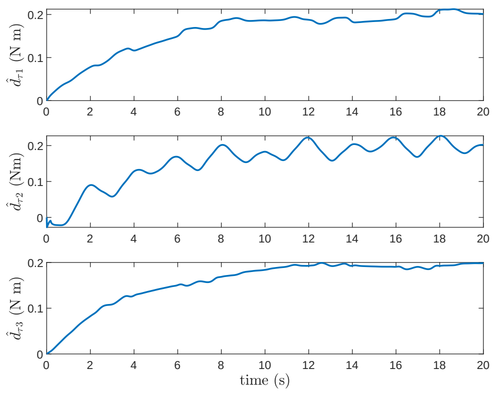

(**d**) Parameter estimates $\hat{d}_\tau$

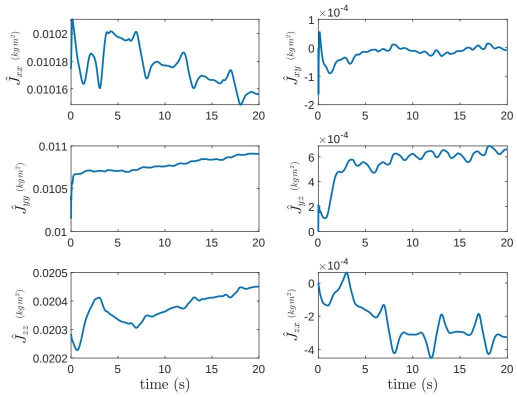

(**e**) Parameter estimates $\hat{J}$

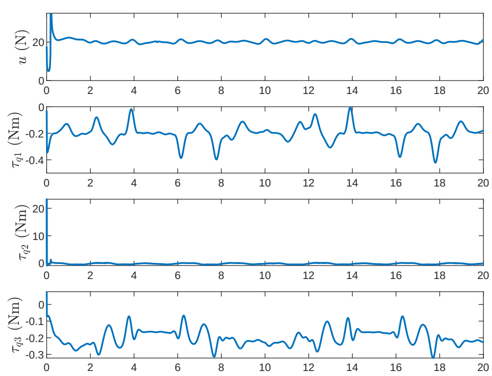

(**f**) Inputs u, τ

Figure 5. Results for the moving arm configuration.

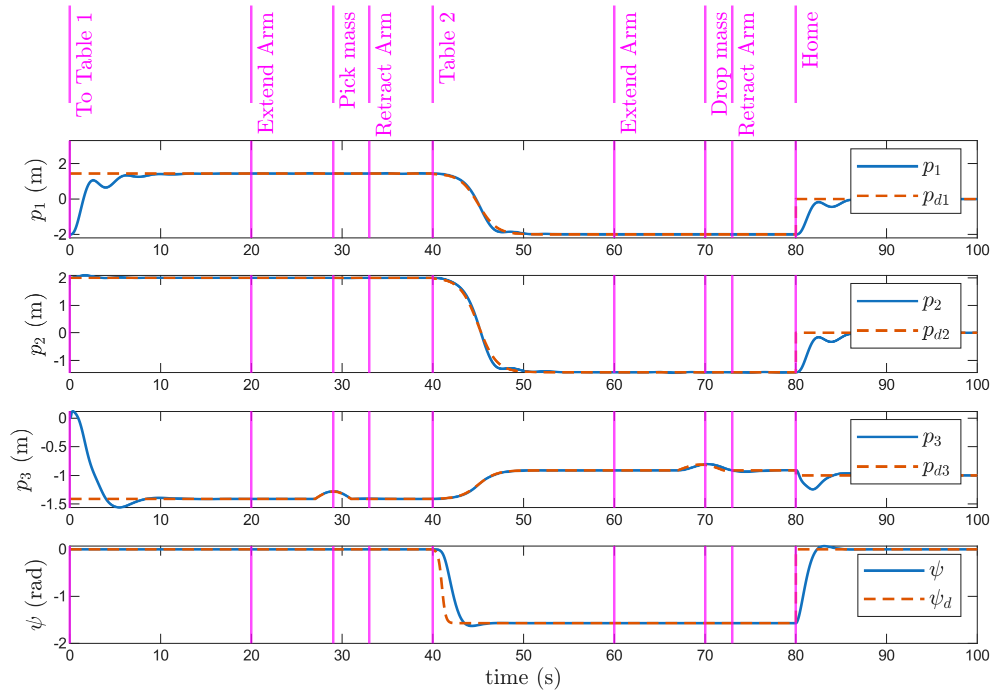

(**a**) UAV pose

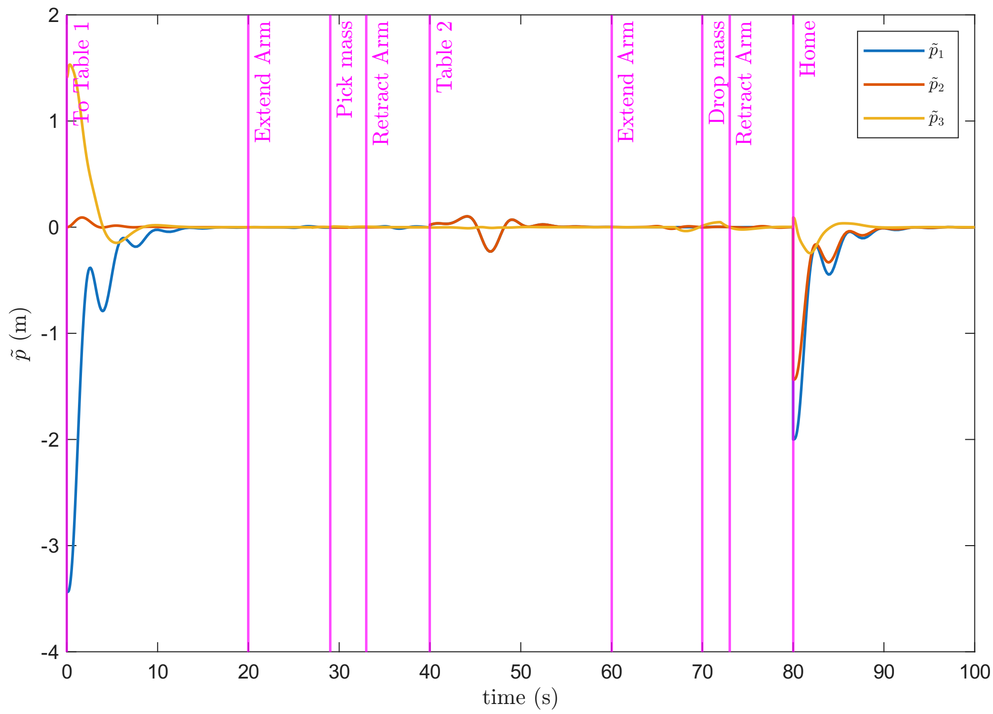

(**b**) Position errors

Figure 6. Pick and place application results: (a) UAV pose and (b) position errors.

Table 4. Object pick and place sequence

Time t	Desired Position p_d	Desired Yaw ψ_d	Arm configuration	Cube Location
0	p_d^1	ψ_d^1	Home	Table 1
20	p_d^1	ψ_d^1	Extending	Table 1
27	$p_d^1 + h(t-27)$	ψ_d^1	Extended	Table 1
29	$p_d^1 + h(t-27)$	ψ_d^1	Extended	UAM
32	p_d^1	ψ_d^1	Retracting	UAM
40	$p_d^1 + \frac{p_d^2 - p_d^1}{1+\exp(-(t-45))}$	$\frac{\psi_d^2}{1+\exp(-(t-45))}$	Home	UAM
60	p_d^2	ψ_d^2	Extending	UAM
67	$p_d^2 + h(t-67)$	ψ_d^2	Extending	UAM
70	$p_d^2 + h(t-67)$	ψ_d^2	Extended	Table 2
73	p_d^2	ψ_d^2	Retracting	Table 2
80	$[0, 0, 0]^T$	0	Home	Table 2

5. Conclusion

In this paper, we have presented a control design for a UAM consisting of a UAV and multi-DoF robotic arm. The design is based on a UAV model that accounts for the arm's effect by including torque and force disturbances and parametric uncertainty. An adaptive backstepping control law is presented that achieves UAV CoM position and yaw tracking when disturbances and parameters are constant. Numerical simulations demonstrate that bounded tracking error results when disturbances and parameters are varying. A practical pick and place task illustrates a case where tracking error converges. Future work involves indoor and output experimental validation of the control with an open source platform as in [30]. An intermediate step for this validation is software-in-the-loop testing that includes various non-idealities such as actuator saturation, sampling effects, state estimation, and rotor drag [31].

References

1. Albers, A.; Trautmann, S.; Howard, T.; .; Frietsch, M.; Sauter, C. Semi-autonomous flying robot for physical interaction with environment. In Proceedings of the 2010 IEEE Conference on Robotics, Automation and Mechatronics, June 2010, pp. 441–446. https://doi.org/10.1109/RAMECH.2010.5513152.
2. Nguyen, H.; Lee, D. Hybrid force/motion control and internal dynamics of quadrotors for tool operation. In Proceedings of the 2013 IEEE/RSJ International Conference on Intelligent Robots and Systems, Nov 2013, pp. 3458–3464. https://doi.org/10.1109/IROS.2013.6696849.
3. Nguyen, H.N.; Ha, C.; Lee, D. Mechanics, control and internal dynamics of quadrotor tool operation. *Automatica* **2015**, *61*, 289 – 301. https://doi.org/https://doi.org/10.1016/j.automatica.2015.08.015.
4. Mersha, A.Y.; Stramigioli, S.; Carloni, R. Variable impedance control for aerial interaction. In Proceedings of the 2014 IEEE/RSJ International Conference on Intelligent Robots and Systems, Sep. 2014, pp. 3435–3440. https://doi.org/10.1109/IROS.2014.6943041.
5. Papachristos, C.; Alexis, K.; Tzes, A. Efficient force exertion for aerial robotic manipulation: Exploiting the thrust-vectoring authority of a tri-tiltrotor UAV. In Proceedings of the 2014 IEEE International Conference on Robotics and Automation (ICRA), May 2014, pp. 4500–4505. https://doi.org/10.1109/ICRA.2014.6907516.
6. Kim, S.; Choi, S.; Kim, H.; Shin, J.; Shim, H.; Kim, H.J. Robust Control of an Equipment-Added Multirotor Using Disturbance Observer. *IEEE Transactions on Control Systems Technology* **2018**, *26*, 1524–1531. https://doi.org/10.1109/TCST.2017.2711602.
7. Jimenez-Cano, A.E.; Martin, J.; Heredia, G.; Ollero, A.; Cano, R. Control of an aerial robot with multi-link arm for assembly tasks. In Proceedings of the 2013 IEEE International Conference on Robotics and Automation, May 2013, pp. 4916–4921. https://doi.org/10.1109/ICRA.2013.6631279.
8. Korpela, C.; Orsag, M.; Pekala, M.; Oh, P. Dynamic stability of a mobile manipulating unmanned aerial vehicle. In Proceedings of the 2013 IEEE International Conference on Robotics and Automation, May 2013, pp. 4922–4927. https://doi.org/10.1109/ICRA.2013.6631280.

9. Kannan, S.; Olivares-Mendez, M.A.; Voos, H. Modeling and Control of Aerial Manipulation Vehicle with Visual sensor. *IFAC Proceedings Volumes* **2013**, *46*, 303 – 309. https://doi.org/10.3182/20131120-3-FR-4045.00053.
10. Kannan, S.; Alma, M.; Olivares-Mendez, M.A.; Voos, H. Adaptive control of Aerial Manipulation Vehicle. In Proceedings of the 2014 IEEE International Conference on Control System, Computing and Engineering (ICCSCE 2014), Nov 2014, pp. 273–278. https://doi.org/10.1109/ICCSCE.2014.7072729.
11. Khalifa, A.; Fanni, M.; Ramadan, A.; Abo-Ismail, A. Modeling and control of a new quadrotor manipulation system. In Proceedings of the 2012 First International Conference on Innovative Engineering Systems, Dec 2012, pp. 109–114. https://doi.org/10.1109/ICIES.2012.6530854.
12. Samadikhoshkho, Z.; Ghorbani, S.; Janabi-Sharifi, F.; Zareinia, K. Nonlinear control of aerial manipulation systems. *Aerospace Science and Technology* **2020**, *104*, 105945. https://doi.org/https://doi.org/10.1016/j.ast.2020.105945.
13. Lippiello, V.; Ruggiero, F. Exploiting redundancy in Cartesian impedance control of UAVs equipped with a robotic arm. In Proceedings of the 2012 IEEE/RSJ International Conference on Intelligent Robots and Systems, Oct 2012, pp. 3768–3773. https://doi.org/10.1109/IROS.2012.6386021.
14. Lippiello, V.; Ruggiero, F. Cartesian Impedance Control of a UAV with a Robotic Arm. In Proceedings of the 10th International IFAC Symposium on Robot Control, 2012, pp. 704–709.
15. Kim, S.; Choi, S.; Kim, H.J. Aerial manipulation using a quadrotor with a two DOF robotic arm. In Proceedings of the 2013 IEEE/RSJ International Conference on Intelligent Robots and Systems, Nov 2013, pp. 4990–4995. https://doi.org/10.1109/IROS.2013.6697077.
16. Yang, H.; Lee, D. Dynamics and control of quadrotor with robotic manipulator. In Proceedings of the 2014 IEEE International Conference on Robotics and Automation (ICRA), May 2014, pp. 5544–5549. https://doi.org/10.1109/ICRA.2014.6907674.
17. Korpela, C.; Orsag, M.; Oh, P. Towards valve turning using a dual-arm aerial manipulator. In Proceedings of the 2014 IEEE/RSJ International Conference on Intelligent Robots and Systems, Sep. 2014, pp. 3411–3416. https://doi.org/10.1109/IROS.2014.6943037.
18. Lee, K.; Back, J.; Choy, I. Nonlinear disturbance observer based robust attitude tracking controller for quadrotor UAVs. *International Journal of Control, Automation and Systems* **2014**, *12*, 1266–1275. https://doi.org/10.1007/s12555-014-0145-x.
19. Bouabdallah, S.; Siegwart, R. Backstepping and Sliding-mode Techniques Applied to an Indoor Micro Quadrotor. In Proceedings of the Proc. IEEE Int. Conf. on Robotics and Automation. IEEE, 2005. https://doi.org/10.1109/robot.2005.1570447.
20. Baraban, G.; Sheckells, M.; Kim, S.; Kobilarov, M. Adaptive Parameter Estimation for Aerial Manipulation. In Proceedings of the Proceedings of the American Control Conference, 2020, pp. 614–619. https://doi.org/10.23919/ACC45564.2020.9147517.
21. Alvarez-Munoz, J.; Marchand, N.; Guerrero-Castellanos, J.F.; Tellez-Guzman, J.J.; Escareno, J.; Rakotondrabe, M. Rotorcraft with a 3DOF Rigid Manipulator: Quaternion-based Modeling and Real-time Control Tolerant to Multi-body Couplings. *International Journal of Automation and Computing* **2018**, *15*, 547–558. https://doi.org/10.1007/s11633-018-1145-8.
22. Petrlík, M.; Báča, T.; Heřt, D.; Vrba, M.; Krajník, T.; Saska, M. A robust UAV system for operations in a constrained environment. *IEEE Robotics and Automation Letters* **2020**, *5*, 2169–2176.
23. Wang, Y.; Lu, Q.; Ren, B. Wind turbine crack inspection using a quadrotor with image motion blur avoided. *IEEE Robotics and Automation Letters* **2023**, *8*, 1069–1076.
24. Moeini, A.; Lynch, A.; Zhao, Q. Disturbance Observer-based Nonlinear Control of a Quadrotor UAV. *Adv. Control Appl.* **2019**, *2*, 1–20.
25. Moeini, A.; Rafique, M.A.; Xue, Z.; Lynch, A.F.; Zhao, Q. Disturbance Observer-Based Integral Backstepping Control for UAVs. In Proceedings of the 2020 International Conference on Unmanned Aircraft Systems (ICUAS), 2020, pp. 382–388.
26. Rafique, M.A. Adaptive Nonlinear Control for Unmanned Aerial Vehicles: Visual Servoing and Aerial Manipulation. Ph.d. thesis, University of Alberta, Edmonton, Alberta, Canada, 2022. https://doi.org/10.7939/r3-rjxg-a163.
27. Bangura, M. Aerodynamics and Control of Quadrotors. PhD thesis, College of Engineering and Computer Science, The Australian National University, 2017.
28. Bouabdallah, S. Design and control of quadrotors with application to autonomous flying. PhD thesis, Ecole Polytechnique Federale de Luasanne, Lausanne, Switzerland, 2007.

 doi:10.20944/preprints202508.1963.v1

29. Khalil, H.K. *Nonlinear Systems*, 3 ed.; Prentice Hall: Upper Saddle River, NJ, 2002.
30. Jiang, Z.; Yu, Y.; Lynch, A. Nonlinear Motion Control of a Multirotor Slung Load System: Experimental Results. In Proceedings of the American Control Conference (ACC), 2024, pp. 2851–2857. https://doi.org/10.23919/ACC60939.2024.10644606.
31. Lawati, M.A.; Zhang, Z.; Yan, E.; Lynch, A.F. Nonlinear Control of a Multi-Drone Slung Load System. In Proceedings of the American Control Conference (ACC), 2025, pp. 1989–1996.